Interplay of charge, spin, and lattice degrees of freedom in the spectral properties of the one-dimensional Hubbard-Holstein model

A. Nocera,[1] M. Soltanieh-ha,[1] C. A. Perroni,[2] V. Cataudella,[2] and A. E. Feiguin[1]

[1]*Department of Physics, Northeastern University, Boston, Massachusetts 02115, USA*
[2]*CNR-SPIN and Dipartimento di Fisica, Università Federico II, Via Cinthia, Napoli I-80126, Italy*

We calculate the spectral function of the one-dimensional Hubbard-Holstein model using the time-dependent density matrix renormalization group, focusing on the regime of large local Coulomb repulsion, and away from electronic half-filling. We argue that, from weak to intermediate electron-phonon coupling, phonons interact only with the electronic charge, and not with the spin degrees of freedom. For strong electron-phonon interaction, spinon and holon bands are not discernible anymore and the system is well described by a spinless polaronic liquid. In this regime, we observe multiple peaks in the spectrum with an energy separation corresponding to the energy of the lattice vibrations (i.e., phonons). We support the numerical results by introducing a well controlled analytical approach based on Ogata-Shiba's factorized wave function, showing that the spectrum can be understood as a convolution of three contributions, originating from charge, spin, and lattice sectors. We recognize and interpret these signatures in the spectral properties and discuss the experimental implications.

I. INTRODUCTION

In the past two decades, we have witnessed a tremendous improvement in the energy and momentum resolution of angle-resolved photoemission spectroscopy (ARPES), which is one of the most powerful experimental tools for investigating strongly correlated materials. In particular, recent ARPES spectra of high-T_C cuprates [1,2], alkali-doped fullerides [3], and manganites [4], have shown that the interplay of electron-electron (e-e) and electron-phonon (e-ph) interactions have an important role in the qualitative and quantitative understanding of the experiments.

When considering systems of low dimensionality, the situation is even more complicated. In one dimension (1D), the low-energy states separate into spin (spinon) and charge (holon) excitations that move with different velocities and are at different energy scales [5–7]. Spin-charge separation has been observed experimentally in semiconductor quantum wires [8], organic conductors [9], carbon nanotubes [10], atomic chains on semiconductor surfaces [11], and recently predicted to be achieved in optical lattices of ultracold atoms [12–14]. A clear detection of the phenomenon has been proposed theoretically in Ref. [15] using time-resolved spin-polarized density measurements. Evidence of spin-charge separation has been observed also in photoemission experiments on quasi-1D cuprate $SrCuO_2$ [16] and on organic conductor TTF-TCNQ [17]. In these quasi-1D materials, the coupling to the lattice is considered to be responsible for the unusual spectral broadening of the spin and charge peaks observed by ARPES. Recently, the interplay between spin, charge, and lattice degrees of freedom has also been investigated in the family of quasi-1D cuprates $Ca_{2+5x}Y_{2-5x}Cu_5O_{10}$, using high resolution resonant inelastic x-ray scattering (RIXS) [18,19].

In 1D systems and in the absence of e-ph interaction, the spin excitations are described by a band whose curvature is proportional to the exchange energy scale J, while the charge excitation dispersion width is comparable to the electronic hopping ($\simeq 4t$). Moreover, the collective excitation spectrum of 1D systems presents spectral weight (shadow bands) at momenta larger than the Fermi momentum k_F due to their Luttinger liquid nature. It is therefore of paramount importance to study the behavior of the photoemission spectrum of materials where it is believed that a strong interaction with the lattice degrees of freedom is present. In particular, this aspect is not entirely understood and one expects that the interplay between e-e and e-ph interactions has a profound effect on spin-charge separation and on the interpretation of the experiments.

The basic lattice model used to describe e-e and e-ph interactions in 1D is the so-called Hubbard-Holstein (HH) Hamiltonian, which contains nearest-neighbor hopping t, on-site Coulomb repulsion U, and a linear coupling between the charge density and the lattice deformation of a dispersionless phonon mode (see Sec. II). Within this model, the electronic spectral properties have been studied by Refs. [20,21], where the adiabatic limit (phonon frequency smaller than the electronic hopping) is mostly analyzed at half electronic filling in the regime of weak to intermediate e-ph coupling. In the first paper, the authors use dynamical density matrix renormalization group (D-DMRG) and assess the robustness of spin-charge separation against e-ph coupling, interpreting the spectral function as a superposition spectra of spinless fermions dressed by phonons. In particular, a peak-dip-hump structure is found, where the dip energy scale is given by the phonon frequency and originated from the charge-mediated coupling of phonons and spinons. In the second paper, the authors use cluster perturbation theory and an optimized phonon approach observing that e-ph coupling mainly gives rise to a broadening of the holon band, due to the presence of many adiabatic phonons.

In contrast to these previous studies, in this paper we consider the case of a phonon frequency larger than the electronic hopping (antiadiabatic limit) and a finite hole doping (or equivalently electronic density below half-filling), a regime that could be currently accessible in the experiments [19]. We develop a controlled analytical approach for the calculation of the spectral function (photoemission spectrum, PES) which is rigorously valid in the presence of an infinitely large Coulomb

repulsion, and in the antiadabatic limit. In this regime, the exchange J is a small energy scale (of the order of t^2/U) in the problem, but it is not zero as in the spinless Holstein model.[1] Our theory relies on Ogata-Shiba's Bethe ansatz solution [34] of the $U \to \infty$ Hubbard model, combined with the Zheng, Feinberg, and Avignon (ZFA) treatment [35] of the e-ph interaction. In order to support the analytical results, we numerically calculate the PES using the time-dependent DMRG [36,37] (tDMRG) finding a quantitative and qualitative agreement with the analytical approximation for weak and strong e-ph interaction. One of the main observations is that the e-ph interaction induces a reduction of the spinon and the holon bandwidths. For strong e-ph interaction, we observe spectral side bands separated by energy gaps with width proportional to the phonon frequency. Eventually, the separation of spin and charge spectral peaks is not appreciable anymore being spinon and holon bands merged in one main band. In this case, the system can be described as a polaronic liquid, with the spectral weight extended well beyond Fermi momentum k_F. The tDMRG simulations show that at weak coupling spin-charge separation is robust against e-ph coupling, and spinon and holon bands are well resolved. Therefore, we argue that, from weak to intermediate e-ph coupling, phonons are mainly coupled to the charge degrees of freedom while the spinon is pretty much unaffected within good approximation. Finally, the PES is investigated with tDMRG decreasing the phonon frequency and exploring also the adiabatic limit. In this case, we reproduce the results of Ref. [20] finding the characteristic spectral peak-dip-hump structure.

The paper is organized as follows: In Sec. II the HH model is briefly introduced. In Sec. III we present an analytical method for calculating the PES, and discuss the validity of the approximations used. In Sec. IV, the numerical results obtained with the tDMRG, and a comparison with the analytical results are discussed. We finally conclude discussing the implications of the results for the experiments.

II. THE 1D HUBBARD-HOLSTEIN MODEL

The HH model describes Einstein phonons locally coupled to electrons described by the Hubbard Hamiltonian. In 1D, it can be written as

$$H = -t \sum_{i,\sigma} (c_{i,\sigma}^\dagger c_{i+1,\sigma} + \text{H.c.}) + U \sum_i n_{i,\uparrow} n_{i,\downarrow}$$
$$+ \omega_0 \sum_i a_i^\dagger a_i + g\omega_0 \sum_{i,\sigma} n_{i\sigma}(a_i + a_i^\dagger), \quad (1)$$

where t is the hopping amplitude between nearest neighbor sites, the total number of lattice sites is L, U is the on-site Coulomb repulsion, ω_0 is the phonon frequency, g is the e-ph coupling constant, $c_{i,\sigma}^\dagger$ ($c_{i,\sigma}$) is the standard electron creation (annihilation) operator on site i with spin $\sigma = \uparrow, \downarrow$, $n_{i,\sigma} = c_{i,\sigma}^\dagger c_{i,\sigma}$ is the electronic occupation operator, and $a_i^\dagger$ (a_i) is the

phonon creation (annihilation) operator. The Planck constant is set to $\hbar = 1$, the lattice parameter $a = 1$, and all of the energies are in the units of the hopping t.

It is well known that the HH model is extremely complicated and impossible to solve analytically. Its phase diagram and ground-state static properties [38–49] have been thoroughly studied in the literature, using different numerical techniques, including DMRG [50–52]. The main difficulty consists of handling the phononic degrees of freedom, which need to be described in principle by an infinite-dimensional Hilbert space at every lattice site. Different truncation schemes for the phononic Hilbert space have been proposed, including the possibility of using optimal phonon bases [53–55]. Still, solving the problem numerically remains remarkably time consuming, especially for the calculation of the dynamical properties such as the spectral function. We remark that a semiclassical treatment of the lattice degrees of freedom has been recently adopted for the study of spectral and transport properties of organic semiconductors [56,57] and the transport properties of suspended carbon nanotubes [58,59]. We point out that throughout the paper, the Coulomb repulsion is considered large enough to avoid competition with other phases such as the charge-density wave Peierls state [38].

III. THE ZFA APPROACH

In this section we present an analytical method that allows us to calculate the photoemission part of the spectral function

$$B(k,\omega) = -\frac{1}{\pi} \text{Im} G(k,\omega) \quad \text{for} \quad \omega < \mu, \quad (2)$$

where $G(k,\omega)$ is the electronic retarded single particle Green's function and μ is the chemical potential. The method consists of a variational canonical transformation originally proposed by Zheng, Feinberg, and Avignon in Ref. [35] and then employed in Ref. [60] for calculating the spectral and optical properties of the spinless Holstein model. The starting point of the approach is the assumption that, in the limit of strong e-ph coupling, $U \to \infty$, and infinity phonon frequency ω_0, the model is described by spinless polarons. Then, the ZFA approach extends the polaron formation to the intermediate e-ph coupling regime, recovering the mean field solution at zero phonon frequency. We introduce the generator of the so-called variational Lang-Firsov transformation [61], given by

$$T[f,\Delta] = e^{g \sum_j [n_j f + \Delta](a_j - a_j^\dagger)}, \quad (3)$$

where $n_j = n_{j,\uparrow} + n_{j,\downarrow}$, and f and Δ are variational parameters whose meaning will be described below. The transformed Hamiltonian is

$$\tilde{H}[f,\Delta] = T^{-1}HT = -t \sum_{i,\sigma} (c_{i,\sigma}^\dagger X_i^\dagger X_{i+1} c_{i+1,\sigma} + \text{H.c.})$$
$$+ (U - 2g^2 f^2 \omega_0) \sum_i n_{i,\uparrow} n_{i,\downarrow} + \omega_0 \sum_i a_i^\dagger a_i$$
$$+ Lg^2 \omega_0 \Delta^2 + g\omega_0(1-f) \sum_i n_i(a_i + a_i^\dagger)$$
$$- g\omega_0 \Delta \sum_i (a_i + a_i^\dagger) + \eta \sum_i n_i, \quad (4)$$

----

[1] In the literature the strong Hubbard-U (U is the on-site Coulomb repulsion) limit of the HH model is usually considered as the spinless Holstein model. For this model, the dynamical properties have been thoroughly studied both analytically and numerically [22–33].

where we have defined a phonon operator $X_i = e^{gf(a_i - a_i^\dagger)}$ and $\eta = g^2\omega_0 f(f-2) + 2g^2\omega_0(f-1)\Delta$. In the next section, we will show the actual procedure employed for the calculation of the variational parameters f and Δ. Also, it will be shown that the variational parameter Δ can be obtained as a function of f [$\Delta = (1-f)N/L$], and one is thus left with only one variational parameter. Assuming $\tilde{f}$ is the optimal choice for f, one can thus proceed by writing the transformed Hamiltonian as

$$\tilde{H}[\tilde{f}] = \tilde{H}_0 + V, \qquad (5)$$

where $\tilde{H}_0$ is the unperturbed part given by strongly correlated electrons and noninteracting phonons,

$$\tilde{H}_0[\tilde{f}] = -te^{-g^2\tilde{f}^2}\sum_{i,\sigma}(c_{i,\sigma}^\dagger c_{i+1,\sigma} + \text{H.c.})$$
$$+ (U - 2g^2\tilde{f}^2\omega_0)\sum_i n_{i,\uparrow}n_{i,\downarrow} + \omega_0\sum_i a_i^\dagger a_i + \tilde{\eta}N$$
$$- g\omega_0(1-\tilde{f})\frac{N}{L}\sum_i(a_i + a_i^\dagger) + g^2\omega_0(1-\tilde{f})^2\frac{N^2}{L}, \qquad (6)$$

with $\tilde{\eta} = g^2\omega_0\tilde{f}(\tilde{f}-2) - 2g^2\omega_0(1-\tilde{f})^2 N/L$, while V is a many-body interaction operator

$$V = -t\sum_{i,\sigma}[c_{i,\sigma}^\dagger(X_i^\dagger X_{i+1} - e^{-g^2\tilde{f}^2})c_{i+1,\sigma} + \text{H.c.}]$$
$$+ g\omega_0(1-\tilde{f})\sum_i n_i(a_i + a_i^\dagger). \qquad (7)$$

The PES is now calculated approximately by neglecting the perturbation V. One can use perturbation theory and consider the effect of V in higher orders of perturbation after the calculation of the PES, but in this paper we are only taking the zeroth order into account. In fact, the determination of the optimal parameter $\tilde{f}$ is meant to minimize the error produced by neglecting the interaction term V from the Hamiltonian (5). The unperturbed Hamiltonian $\tilde{H}_0[\tilde{f}]$ still contains information about e-ph interacting terms in the original Hamiltonian (1), since all the parameters of $\tilde{H}_0[\tilde{f}]$ are renormalized by our variational technique. Indeed, $\tilde{H}_0[\tilde{f}]$ consists of free phonons and a Hubbard model with a shift $\tilde{\eta}$ of the chemical potential, a hopping $\tilde{t}$, and an on-site repulsion $\tilde{U}$ renormalized by the e-ph interaction

$$\tilde{t} = te^{-g^2\tilde{f}^2}, \quad \tilde{U} = U - 2g^2\tilde{f}^2\omega_0. \qquad (8)$$

In this limit, in the transformed space electronic and lattice degrees of freedom are governed by independent Hamiltonians

$$\tilde{H}_0[\tilde{f}] = \tilde{H}_{\text{el}} + \tilde{H}_{\text{phonon}}, \qquad (9)$$

and the total wave function can be factorized in two parts:

$$|\psi\rangle = |\Lambda\rangle \otimes |\{n_{\text{ph}}\}\rangle, \qquad (10)$$

where $|\Lambda\rangle$ describes the electrons, and $|\{n_{\text{ph}}\}\rangle$ is given by the product of L separate noninteracting phononic wave functions, each one containing an integer number of phonons ($|\{n_{\text{ph}}\}\rangle = |\{n_{\text{ph}}^0\}\rangle \otimes |\{n_{\text{ph}}^1\}\rangle \otimes \cdots |\{n_{\text{ph}}^{L-1}\}\rangle$). It is trivial to show that the PES in the original space is now given by

$$B(k,\omega) = \sum_{\tilde{n}}|\langle\tilde{n}|X_0|0\rangle|^2 B_e(k,\omega+\tilde{n}\omega_0), \qquad (11)$$

where $B_e(k,\omega)$ is the PES in the transformed space and the sum is extended over all the phonon states $\tilde{n}$ of a single site phonon. $B_e(k,\omega)$ is now evaluated in the Lehmann representation

$$B_e(k,\omega) = L\sum_{z,\sigma}|\langle z,N-1|c_{k,\sigma}|\text{GS},N\rangle|^2$$
$$\times \delta(\omega - E_{\text{GS}}^N + E_z^{N-1}), \qquad (12)$$

where $c_{k,\sigma}$ destroys an electron with momentum k and spin σ ($c_{j,\sigma} = \frac{1}{\sqrt{L}}\sum_{k'}e^{ik'j}c_{k',\sigma}$), N is the total number of electrons, and z the final state with $N-1$ electrons. E_z^{N-1} represents the total energy of the final state, and E_{GS}^N describes the energy of the ground state of the original Hamiltonian (1) with N electrons. Since Einstein phonons carry no momentum, we can impose the momentum conservation with the term $\delta_{k,P_{\text{GS}}^N - P_z^{N-1}}$ to reduce Eq. (12) to a calculation involving only site 0 in the real space and one phonon mode at that site:

$$B_e(k,\omega) = L\sum_{z,\sigma}|\langle z,N-1|c_{0,\sigma}|\text{GS},N\rangle|^2$$
$$\times \delta(\omega - E_{\text{GS}}^N + E_z^{N-1})\delta_{k,P_{\text{GS}}^N - P_z^{N-1}}. \qquad (13)$$

Up to here, no assumptions have been made on the electronic spectral function and the general form shown above is extremely complex. However, in the limit of $\tilde{U} \gg \tilde{t}$ one can use Ogata-Shiba's factorization [34] to show that the electronic wave function $|\Lambda\rangle$ in Eq. (10) is split into spin and charge parts. The total wave function $|\psi\rangle$ can be therefore factorized as

$$|\psi\rangle = |\phi\rangle \otimes |\chi\rangle \otimes |\{n_{\text{ph}}\}\rangle, \qquad (14)$$

where $|\phi\rangle$ describes spinless charges and $|\chi\rangle$ is the spin wave function that corresponds to a "squeezed" chain of N spins, where all the unoccupied sites have been removed. In this limit, charge, spin, and lattice degrees of freedom are governed by independent Hamiltonians

$$\tilde{H}_0[\tilde{f}] = \tilde{H}_{\text{charge}} + \tilde{H}_{\text{spin}} + \tilde{H}_{\text{phonon}}. \qquad (15)$$

Due to this simplification, we are now able to tackle the problem and calculate the PES. Indeed, operator $c_{0,\sigma}$ after the polaron transformation will look like $c_{0,\sigma}X_0$. Moreover, using the Ogata Shiba's formalism [34] one can factorize the electronic annihilation operator $c_{0,\sigma}$ as $c_{0,\sigma} = Z_{0,\sigma}b_0$, where b_0 is a spinless fermionic operator acting on the (spinless) charge part of the wave function $|\phi\rangle$, and $Z_{0,\sigma}$ is acting on the spin part $|\chi\rangle$. The $Z_{0,\sigma}$ operator has a very peculiar behavior, destroying the spin σ at site $i = 0$ as well as the site, making the chain $L-1$ sites long. For details about the use of the $Z_{0,\sigma}$ operator we refer the reader to Refs. [62–64]. The spectral function can be therefore expressed as a convolution

$$B_e(k,\omega) = \sum_{\omega',Q,\sigma}D_\sigma(Q,\omega')B_Q(k,\omega-\omega'), \qquad (16)$$

where $D_\sigma(Q,\omega)$ is the spin spectral function with momentum Q, and

$$B_Q(k,\omega) = L\sum_{\{I\}}|\langle\psi_{L,Q}^{N-1}\{I\}|b_0|\psi_{L,\pi}^{N,\text{GS}}\rangle|^2$$
$$\times \delta(\omega - E_{\text{GS}}^N + E_z^{N-1})\delta_{k,P_{\text{GS}}^N - P_z^{N-1}} \qquad (17)$$

describes the charge part. By following the approach introduced in Ref. [62], one can calculate numerically both $D_\sigma(Q,\omega)$ and $B_Q(k,\omega)$.

A. Variational calculation of the parameter f

In this section we determine the variational parameters f and Δ appearing in the transformed Hamiltonian (4) of the previous section. An effective electronic Hamiltonian, H_{eff}, is used, which is obtained by averaging Eq. (4) on the phononic vacuum of the transformed Hilbert space, $H_{\text{eff}}[f,\Delta] = \langle O_{\text{ph}}|\tilde{H}|O_{\text{ph}}\rangle$,

$$H_{\text{eff}}[f,\Delta] = -te^{-g^2 f^2}\sum_{i,\sigma}(c^\dagger_{i,\sigma}c_{i+1,\sigma} + \text{H.c.})$$

$$+ (U - 2g^2 f^2\omega_0)\sum_i n_{i,\uparrow}n_{i,\downarrow}$$

$$+ \eta\sum_i n_i + Lg^2\omega_0\Delta^2. \qquad (18)$$

The parameter Δ is simply obtained by using the Hellmann-Feynman theorem

$$\frac{\partial}{\partial\Delta}\langle\text{GS}_{\text{eff}}|H_{\text{eff}}|\text{GS}_{\text{eff}}\rangle = 0 \Rightarrow \Delta = (1-f)\frac{N}{L},$$

where N is the total number of electrons, N/L is the electronic density, and $|\text{GS}_{\text{eff}}\rangle$ is the ground state of H_{eff}. One is now left only with the determination of the parameter f, which will be found by solving the Hamiltonian

$$H_{\text{eff}}[f] = -te^{-g^2 f^2}\sum_{i,\sigma}(c^\dagger_{i,\sigma}c_{i+1,\sigma} + \text{H.c.})$$

$$+ (U - 2g^2 f^2\omega_0)\sum_i n_{i,\uparrow}n_{i,\downarrow}$$

$$+ g^2\omega_0(1-f)^2 N^2/L + \eta N, \qquad (19)$$

by using the static DMRG and minimizing the ground-state energy of this new Hamiltonian as a function of f. For each set of values U, t, g, and ω_0, one can obtain an optimal polaronic parameter $\tilde{f}$. In Fig. 1(a), the ground-state energy of $H_{\text{eff}}[f]$ as a function of f for two different values of e-ph coupling $g = 0.8$ and $g = 1.8$ is shown. Here $N/L = 0.75$, $U = 20$, and $\omega_0 = 2.0$. For $g = 1.8$ the value of $\tilde{f}$ obtained is close to 0.8 meaning that for these sets of parameters the system is near the polaronic regime, which ideally is expected to be reached for stronger e-ph coupling and phonon frequency. Indeed, for $\tilde{f} = 1$ one has well-defined polarons, while, for $\tilde{f} = 0$, the unitary transformation, Eq. (3), becomes trivially the identity. In Fig. 1(b), the optimal polaronic parameter $\tilde{f}$ as a function of e-ph is shown. As will become clear in the next section, $\tilde{f}$ describes the degree of polaron formation, which is the amount of spectral weight redistribution in phonon side bands.

B. Analytical results

Once the *optimal* $\tilde{f}$ is determined, one can finally study and analyze the properties of the PES calculated from Eqs. (16) and (11). We start by considering a phonon frequency $\omega_0 > 1$ (antiadiabatic limit) and choose, in particular, $\omega_0 = 2.0$. Moreover, throughout this paper, we consider an electronic
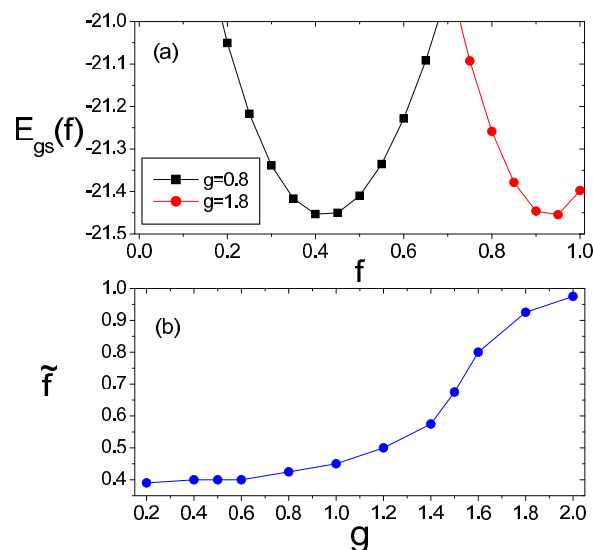
FIG. 1. (Color online) The parameter $\tilde{f}$ is obtained by minimizing the ground-state energy of Hamiltonian (19) with respect to f. Panel (a) shows DMRG calculations for two different values of e-ph coupling g (the potential curve obtained for $g = 1.8$ has been shifted in energy by an arbitrary constant, which is irrelevant in our description where only the position of the minimum is important). Panel (b) shows $\tilde{f}$ as a function of g. All results are for density $N/L = 0.75$.

filling equal to $N/L = 0.75$. Figure 2 shows $B(k,\omega)$ from weak e-ph coupling $g = 0.2$ up to strong interaction $g = 2.0$. In order to interpret the results in more detail, Fig. 3 is showing three vertical cuts at $k = 0$, $k = k_F$ ($k_F = \pi N/2L = 0.375\pi$), and $k = 2k_F$ of the same spectrum [dashed (red) lines]. We note that the spectrum for $g = 0.2$ is very similar to the $g = 0$ PES (not shown): The presence of spin-charge separation is evident [20,21,65], where the spectral weight concentrated on the spinon and holon bands forming a triangular spectral structure between $-k_F$ and $+k_F$ (Fig. 2). As expected for a Luttinger liquid, the shadow bands extend beyond k_F. A closer look at the cuts in Fig. 3 in this weak-coupling regime, shows that phonon effects are negligible: One can observe clearly the higher spinon peak at the top of the spectrum (at $\omega - \mu \simeq -0.05$ for $k = k_F$), and a shifted holon peak.

At $g = 0.6$, phonon effects start to become appreciable with interesting features at all momenta. One can observe a reduction of the spinon and holon bandwidth, as the triangular spectral structure comprising the spinon and holon bands gets *squeezed*. Indeed, the reduction of the spinon and holon bandwidths is due to the fact that the e-ph coupling renormalizes the hopping parameter $\tilde{t} = te^{-g^2\tilde{f}^2}$ exponentially [see Hamiltonian $H_0[\tilde{f}]$, Eq. (5)]. Moreover, one starts to see a *replica* of the entire spectrum appearing shifted below the main band by an energy amount exactly equal to the phonon frequency ω_0. As one can observe in Fig. 1, for the set of parameters used in this paper $\tilde{f}$ assumes a value of 0.4 for $g = 0.2$ increasing slightly up to 0.5 for $g = 1.2$, pointing out that strong Coulomb repulsion and the large phonon frequency already give a sizable spectral redistribution from weak to intermediate e-ph couplings.
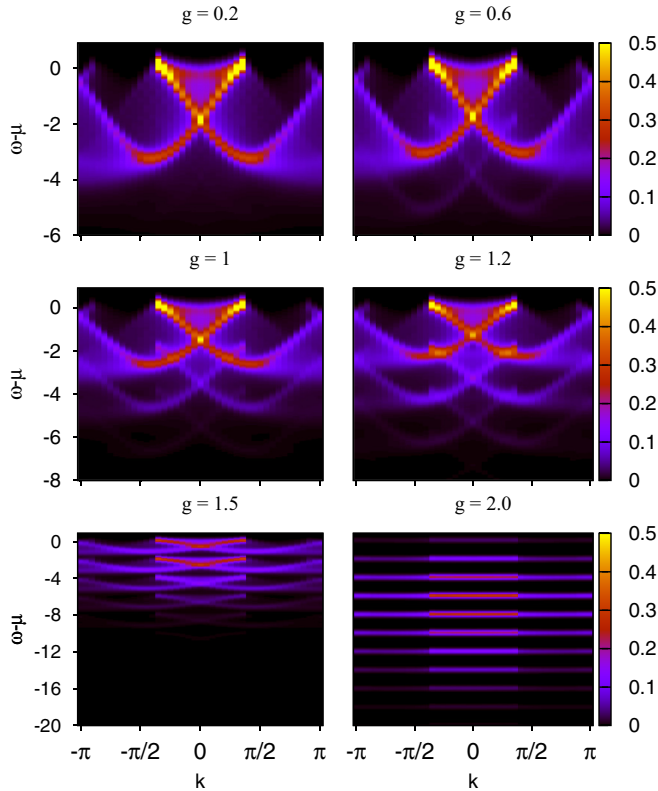
FIG. 2. (Color online) Photoemission spectrum calculated with the ZFA method in the antiadiabatic regime ($\omega_0 = 2.0$) for different e-ph couplings $g = 0.2, 0.6, 1.0, 1.2, 1.5, 2.0$. Here $L = 32$ sites, $U = 20$, and filling $N/L = 3/4$.

Increasing the e-ph coupling, the spectral weight redistribution in identical replicas continues (see panels $g = 1.0$, $g = 1.2$, and $g = 1.5$ of Fig. 2), until the triangular structure is almost collapsed into a flat line for $g = 1.5$. Moreover, For $g \leqslant 1.5$, the PES is broken in spectral replicas (at least five for
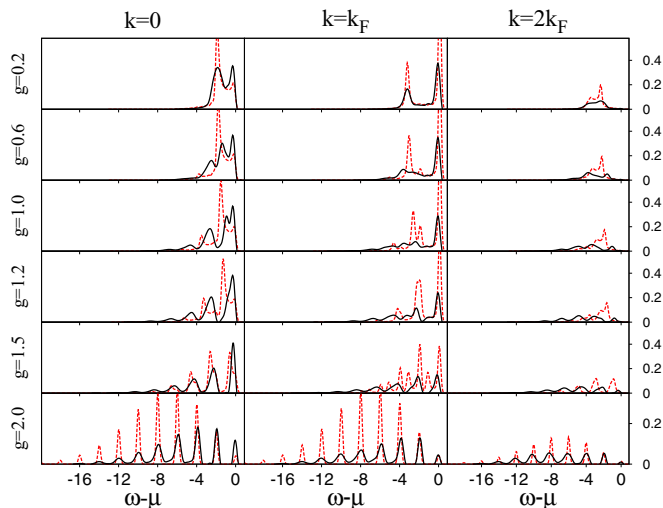
FIG. 3. (Color online) Three cuts at $k = 0, k_F, 2k_F$ of photoemission spectrum calculated with the ZFA approach [dashed (red) line] and using the tDMRG [solid (black) line].

$g = 1.5$) whose weight decreases from the first structure to the following's. This is not true anymore for the case of $g = 2.0$. In this case, one can observe more than ten spectral replica lines with a Gaussian distribution of the spectral weights typical of the polaronic regime [66]. In this case, the separation between the holon and the spinon peak is not discernible anymore, suggesting that the system is in a state that can be described in terms of a spinless polaronic liquid where the spins are completely uncorrelated. It is now clear that the quantity f governs the magnitude of the antiadiabatic polaronic effect, which mainly consists in a spectral redistribution in phonon replicas. It is important to point out that it also provides a shift of the chemical potential given by the quantity $\tilde{\eta} = g^2\omega_0\tilde{f}(\tilde{f} - 2) + 2g^2\omega_0(\tilde{f} - 1)\Delta$. All the spectra shown in Fig. 2 are shifted by correct chemical potential μ calculated with static DMRG ($\mu = E_{N+1} - E_N$, where E_m is the ground-state energy of the system with m particles) and furthermore displaced by $\tilde{\eta}$, a quantity that increases quadratically as a function of the variational parameter $\tilde{f}$ as the e-ph is increased.

In the next section we present a numerical calculation of the PES with the tDMRG, which will allow us to verify and support the results of the ZFA approach.

IV. SPECTRAL FUNCTION WITH tDMRG

In order to obtain dynamical properties of 1D quantum lattice models in the presence of phonons, several techniques such as dynamical DMRG [20] and exact diagonalization combined with cluster perturbation theory have been used in the literature [21]. In contrast to these approaches, here the PES is calculated using the tDMRG with Krylov expansion of the time-evolution operator [67–71]. The time evolution is computed using $m = 400$ DMRG states and the bare phonon bases are truncated keeping up to nine phonons per site. Unless otherwise stated, a lattice with $L = 32$ sites, $N = 24$ electrons, and open boundary conditions is considered. In order to calculate the PES, we measure the time-dependent correlation function

$$B_{i,j}(t) = i\langle\Psi_0|e^{iHt}c_i^\dagger e^{-iHt}c_j|\Psi_0\rangle, \qquad (20)$$

where $|\Psi_0\rangle$ is the ground state of Hamiltonian (1). $|\Psi_0\rangle$ and the ground-state energy are calculated using static DMRG. Excited states $|\Psi_j\rangle = c_j|\Psi_0\rangle$ and their time evolution $|\Psi_j(t)\rangle = e^{-iHt}|\Psi_j\rangle$ are then calculated with the tDMRG. Since the time evolution of the ground state is trivial $\langle\Psi_0|e^{iHt} = e^{iE_{GS}t}\langle\Psi_0|$, Eq. (20) reduces to

$$B_{i,j}(t) = ie^{iE_{GS}t}\langle\Psi_0|c_i^\dagger|\Psi_j(t)\rangle, \qquad (21)$$

which has been calculated for all pairs (i,j) with $i,j = 0$, $L - 1$. Long time evolutions up to $T_{end} = 14$ with time steps of $\Delta t = 0.01$ are considered, and $B(k,\omega)$ is obtained by a space-time Fourier transform performed using a Hann window function [$H(x) = \frac{1}{2}[1 + \cos(x\pi)]$ with $x = 2t/T_{end}$], giving a broadening of the spectral peaks approximately given by $\delta \simeq 0.25$ (the details of the procedure are reported in Refs. [36,72]). Here, k and ω are the momentum and energy of the electron.
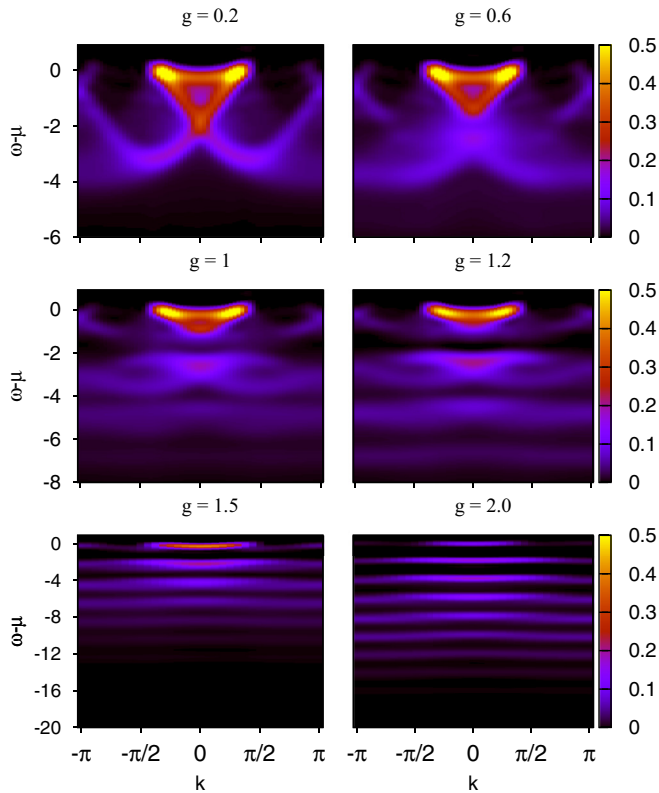
FIG. 4. (Color online) Photoemission spectrum of the HH model calculated with tDMRG for the same frequency and e-ph coupling values considered in Fig. 2. Here $L = 32$ sites, $U = 20$, and filling $N/L = 3/4$.

A. Numerical results

Figure 4 shows the PES calculated with the tDMRG in the antiadiabatic regime, for the same regime of parameters of Fig. 2. In analogy with the results obtained with the ZFA approach, we also show three vertical cuts of the spectrum at $k = 0$, $k = k_F$, and $k = 2k_F$ in Fig. 3 [solid (black) lines]. It is important to point out that, even within the ZFA approach, a broadening of the spectral peaks of the order of $\delta \simeq 0.25$ has been used.

As stated in the previous section, one expects that the ZFA approach is a good approximation of the results in the regime where $\tilde{U} \gg \tilde{t}$ and $\omega_0 > \tilde{t}$. In particular, as one can see in the top row of panels of Fig. 3, for $g = 0.2$ a very good agreement between ZFA and the tDMRG results is obtained. This characteristic is also evident at all momenta if one looks at the upper left panels of Figs. 4 and 2.

Noticeable differences between the ZFA approach and the tDMRG results can be observed in the intermediate e-ph coupling regime ($g = 0.6, 1.0, 1.2$). In this case, the ZFA approach is qualitatively reproducing the reduction of the spinon and holon bandwidths, which are parametrized by the renormalized hopping parameter $\tilde{t} = t e^{-g^2 \tilde{f}^2}$ in the Hamiltonian $H_0[\tilde{f}]$, Eq. (5). While reproducing the correct position of the spectral side bands, the ZFA approach provides access to their internal structure, showing that the separation between the holon and spinon peaks is still well defined.

For $g = 0.6$, tDMRG results show an apparent suppression of the spectral weight or gap seems to appear at $\omega - \mu \simeq -2$ with the formation of a new band ranging from $\omega - \mu \simeq -2$ to $\omega - \mu \simeq -4$, whose dispersion resembles those of the holon and shadow bands. The same characteristics are visible in Fig. 3 for $k = 0$, where the distance between the spinon peak and the holon peak is reduced and a side band at the left of the holon peak is formed. This new spectral feature seems to originate from the holon band, while the height of the spinon peak is practically unchanged going from $g = 0.2$ to $g = 0.6$.

At $g = 1.0$, the progressive reduction of the electronic bandwidth (both of the spinon and holon bands) is even more evident, and the triangular spectral structure has almost collapsed. The new band formed at $g = 0.6$ is now separated by a larger gap with respect to the main spectrum, while the spectral redistribution creates a newer side band whose width is smaller and ranging from $\omega - \mu \simeq -4$ to $\omega - \mu \simeq -6.2$. As one can see, in Fig. 3 for $k = 0$, several side bands separated in energy by a quantity proportional to ω_0 are visible. The side bands present no internal structure and suggest that, up to $g = 1.0$, they originate from the holon bands without contribution from the spinons. These results indicate that, from weak to intermediate g, spin-charge separation is robust against e-ph coupling: The phonons couple mainly with charge degrees of freedom, leaving the spinon band almost unaffected.

For $g = 1.2$, the original triangular feature in the PES is completely collapsed to a flat structure. Also, if one looks at Fig. 3 for $k = 0$ and $k = k_F$ for the same value of g, the height of the first spectral peak is dramatically increased with respect to the case of $g = 1.0$. This indicates that one is entered in the strong e-ph coupling regime where the main band is followed by many side bands coming from both holon *and* spinon bands. This description, as one can see in Fig. 4, is even more evident for $g = 1.5$, where the PES is broken in spectral lines whose weight decreases from the first structure to the following's and extends beyond the Fermi momentum k_F. Besides, the separation between the holon and the spinon peak is not discernible anymore, suggesting that the system is going towards a state that can be described in terms of a spinless polaronic liquid where the spins are completely uncorrelated. Indeed, for $g = 2.0$, the physics of phonon side bands is dominating the PES, observing several spectral structures have a smaller width (compared to $g = 1.5$ results), bigger height, and that the first spectral structure has less weight than the second one.

At strong e-ph coupling, the ZFA approach provides $\tilde{f} = 0.675$ for $g = 1.5$ and $\tilde{f} = 0.975$ for $g = 2.0$. In these cases, the PES calculated within the ZFA approach gives the same number of phonon side bands with widths and heights of the same order of magnitude of the tDMRG results. Moreover, tDMRG results automatically contain information about the shift in the chemical potential mentioned in the previous section. The optimal shift given by the ZFA approach is in total agreement with the chemical potential calculated with static DMRG in the entire range of e-ph couplings. Strikingly, the ZFA approach is giving qualitatively the same nonzero spectral weight distribution at momenta larger than k_F, confirming that, in this case, the system can be described as a polaron liquid.

In order to further investigate this behavior, we have studied the ground-state momentum distribution function
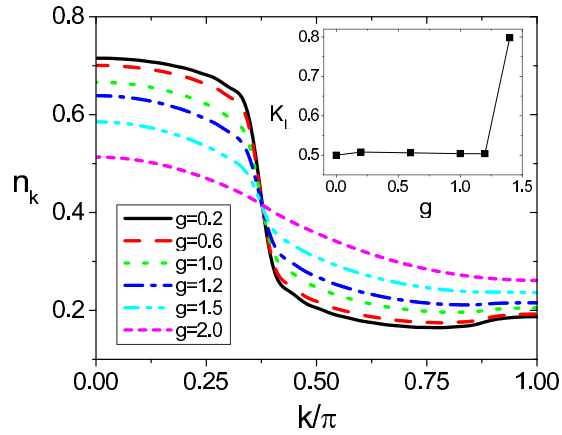
FIG. 5. (Color online) Momentum distribution function for the same parameter values as in Fig. 4. Solid (black), dashed (red), dotted (green), dashed-dotted (blue), dashed-dotted-dashed (cyan), short-dashed (magenta), represent respectively $g = 0.2, 0.6, 1.0, 1.2, 1.5, 2.0$. Inset: Luttinger parameter K as a function of g, extracted from the electronic density-density correlation function.

FIG. 6. (Color online) Panels (a) and (b) show the spin-spin correlation function from the center of the chain for different g's in logarithmic (absolute value) and linear scale, respectively. Inset of panel (a): slope of a linear fit for the spin-spin correlation in logarithmic scale.

$n_k = (1/L) \sum_{i,j} e^{-ik(i-j)} \langle c_i^\dagger c_j \rangle$ and the spin-spin correlation function in real space, $\langle S_z(L/2)S_z(L/2+i) \rangle$, from the center of the chain. As expected for correlated 1D systems, the momentum distribution function shown in Fig. 5 presents a smooth crossover at the Fermi momentum k_F for all e-ph coupling values. We point out that the e-ph coupling reduces the decrease at k_F and, globally, it broadens the momentum distribution function. Eventually, for $g = 2.0$, one gets an almost flat profile with $n_{k=0} \simeq 0.45$ and $n_{k=\pi} \simeq 0.325$. In the inset of Fig. 5, the Luttinger parameter K extracted from the density-density correlation function slope at small momentum [73] is plotted as a function of the e-ph interaction. According to Luttinger liquid theory [74], in the weak e-ph coupling regime one has $K = 1/2$ as in the $U \to \infty$ limit without phonons. By increasing the e-ph interaction, K remains constant and equal to $1/2$ up to $g = 1.2$, and then increases because the e-ph coupling reduces the effective e-e interaction ($\tilde{U} = U - 2g^2\omega_0$).

In Fig. 6, the spin-spin correlations as a function of the distance from the center of the chain is shown both in logarithmic [panel (a)] and in linear scale [panel (b)]. In the first case, it decreases linearly and its slope is decreasing as a function of the e-ph interaction [see inset of panel (a)]. Up to $g = 1.6$, spin-spin correlations decay approximately with the same behavior. For $g > 1.6$, one observes a smooth crossover towards a polaronic regime where spin degrees of freedom are completely uncorrelated and correlations decay faster and faster with respect to distance from the center of the system [see panel (b)].

B. tDMRG results for intermediate e-ph coupling

In this section, we extend the analysis by discussing the tDMRG results for intermediate e-ph coupling $g = 1.0$, as a function of the phonon frequency ω_0. The results are shown in Fig. 7. For $\omega_0 = 0.5$, we observe a behavior different from that discussed in the previous section. For instance, at $k = 0$, a dip structure at the left side of the spinon peak is shifted
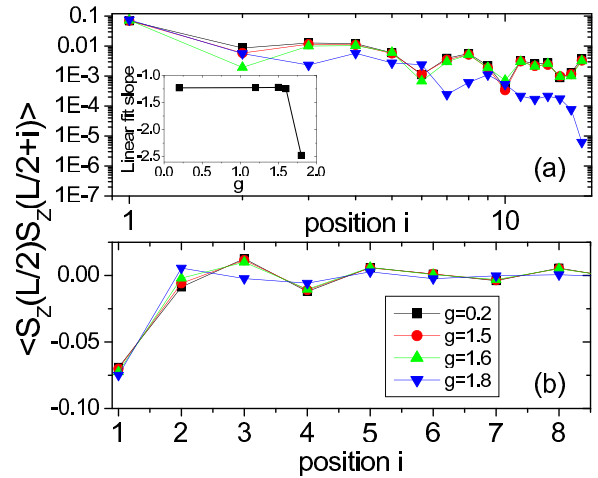
by a quantity equal to $\omega_0 = 0.5$, reproducing qualitatively the results discussed in Ref. [20]. In this reference, the PES is constructed by a superposition of a set of holon dispersions forming a cosine band with width $4t$ in the absence of e-ph interaction. Moreover, each holon dispersion is characterized by one spinon momentum. In the presence of e-ph interaction, due to spin-charge separation each holon couples with phonons independently and the PES is interpreted as a spectrum of spinless electrons dressed by Einstein phonons. This generates a split of the holon dispersion that is away from the top of the spectrum by a shift equal to ω_0, and a transfer of spectral weight to high energy giving a characteristic peak-dip-hump structure. Our results are consistent with this picture, confirming that
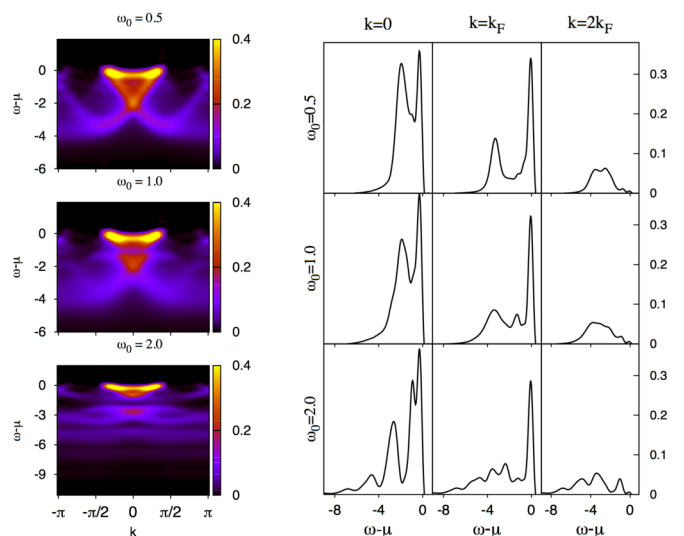
FIG. 7. (Color online) Panel (a) shows the photoemission spectrum for $g = 1.0$, and different phonon frequencies $\omega_0 = 0.5, 1.0, 2.0$. Panel (b) shows three cuts at $k = 0$, $k = k_F$, and $k = 2k_F$ of the photoemission spectrum reported in panel (a).

spin-charge separation is robust in this regime. In contrast to what was discussed in the previous section for $\omega_0 = 2.0$, where polaronic effects dominate and the phonon frequency is smaller than the hopping t, the e-ph coupling effect gives rise to a dip in between the holon and spinon peak. Moreover, this dip structure in the spectrum shifts by an energy proportional to ω_0 [see panel (b) of Fig. 7 for $\omega_0 = 1.0$ and $k = 0$]. In this case, our data shows also a shoulder on the left side of the holon peak, in contrast to what was found in Ref. [20]. In our calculation, this feature can be interpreted as the onset of phonon side bands. Increasing the phonon frequency to $\omega_0 = 2.0$, several sidebands in the PES are found as discussed in the previous section. Interestingly, at $k = k_F$, instead of a dip we find a peak separated from the spinon band by an energy difference equal to ω_0. Eventually, at the Fermi momentum and for larger frequencies, these features become part of the first and the higher side bands.

V. CONCLUSION

We have studied the spectral function of the 1D HH model using the tDMRG method, in the limit of large Coulomb repulsion, and away from electronic half-filling. The entire range of the e-ph coupling has been studied. Our results indicate that from weak to intermediate g spin-charge separation is robust against e-ph coupling: The phonons couple mainly with the charge degrees of freedom, leaving the spinon band almost unaffected. For sufficiently strong e-ph interaction, the PES weight is redistributed in phonon side bands, and the spinon and holon spectral features are not discernible anymore. In this regime, we support the numerical tDMRG results with an analytical calculation, determining variationally the amount of spectral redistribution and approximating the wave function as a convolution of charge, spin, and phonon parts. In this case, a very good qualitative and quantitative agreement with tDMRG results is obtained, and the system can be described as a polaronic liquid, with nonzero spectral weight at momenta larger than the Fermi momentum. We can now briefly discuss the results described above making a contact with the experiments described in Ref. [18]. In this paper, the authors measure the RIXS spectra of a family of quasi-1D cuprates $Ca_{2+5x}Y_{2-5x}Cu_5O_{10}$, an insulating system that can be doped over a wide range of hole concentrations. The experiment reveals a phonon with energy equal to 70 meV (a quantity larger than the typical transfer hopping t along the chains in quasi 1-D cuprates) strongly coupled to the electronic state at different hole dopings. It is found that the spectral weight of phonon excitations in the RIXS spectrum is directly dependent on the e-ph coupling strength and doping, producing multiple peaks in the spectrum with an energy separation corresponding to the energy of the quanta of the lattice vibrations, in a fashion similar to what we obtain in the present paper. We believe that, even in the ARPES spectra of these materials, phonon side-band structures could be experimentally observable in the PES.

[1] A. Lanzara, P. Bogdanov, X. Zhou, S. Kellar, D. Feng, E. Lu, T. Yoshida, H. Eisaki, A. Fujimori, K. Kishio *et al.*, Nature (London) **412**, 510 (2001).

[2] G.-H. Gweon, T. Sasagawa, S. Zhou, J. Graf, H. Takagi, D.-H. Lee, and A. Lanzara, Nature (London) **430**, 187 (2004).

[3] O. Gunnarsson, Rev. Mod. Phys. **69**, 575 (1997).

[4] A. Lanzara, N.-L. Saini, M. Brunelli, F. Natali, A. Bianconi, P.-G. Radaelli, and S.-W. Cheong, Phys. Rev. Lett. **81**, 878 (1998).

[5] A. O. Gogolin, A. A. Nersesyan, and A. M. Tsvelik, *Bosonization and Strongly Correlated Systems* (Cambridge University Press, Cambridge, 2004).

[6] T. Giamarchi, *Quantum Physics in One Dimension* (Clarendon Press, Oxford, 2004).

[7] V. V. Deshpande, M. Bockrath, L. I. Glazman, and A. Yacoby, Nature (London) **464**, 209 (2010).

[8] O. Auslaender, H. Steinberg, A. Yacoby, Y. Tserkovnyak, B. Halperin, K. Baldwin, L. Pfeiffer, and K. West, Science **308**, 88 (2005).

[9] T. Lorenz, M. Hofmann, M. Grüninger, A. Freimuth, G. Uhrig, M. Dumm, and M. Dressel, Nature (London) **418**, 614 (2002).

[10] M. Bockrath, D. H. Cobden, J. Lu, A. G. Rinzler, R. E. Smalley, L. Balents, and P. L. McEuen, Nature (London) **397**, 598 (1999).

[11] C. Blumenstein, J. Schäfer, S. Mietke, S. Meyer, A. Dollinger, M. Lochner, X. Cui, L. Patthey, R. Matzdorf, and R. Claessen, Nat. Phys. **7**, 776 (2011).

[12] C. Kollath, U. Schollwöck, and W. Zwerger, Phys. Rev. Lett. **95**, 176401 (2005).

[13] C. Kollath and U. Schollwck, New J. Phys. **8**, 220 (2006).

[14] A. E. Feiguin and D. A. Huse, Phys. Rev. B **79**, 100507 (2009).

[15] T. Ulbricht and P. Schmitteckert, Europhys. Lett. **86**, 57006 (2009).

[16] B. Kim, H. Koh, E. Rotenberg, S.-J. Oh, H. Eisaki, N. Motoyama, S. Uchida, T. Tohyama, S. Maekawa, Z.-X. Shen *et al.*, Nat. Phys. **2**, 397 (2006).

[17] M. Sing, U. Schwingenschlögl, R. Claessen, P. Blaha, J.-P.-M. Carmelo, L.-M. Martelo, P.-D. Sacramento, M. Dressel, and C. S. Jacobsen, Phys. Rev. B **68**, 125111 (2003).

[18] W. S. Lee, S. Johnston, B. Moritz, J. Lee, M. Yi, K. J. Zhou, T. Schmitt, L. Patthey, V. Strocov, K. Kudo *et al.*, Phys. Rev. Lett. **110**, 265502 (2013).

[19] J. J. Lee, B. Moritz, W. S. Lee, M. Yi, C. J. Jia, A. P. Sorini, K. Kudo, Y. Koike, K. J. Zhou, C. Monney *et al.*, Phys. Rev. B **89**, 041104 (2014).

[20] H. Matsueda, T. Tohyama, and S. Maekawa, Phys. Rev. B **74**, 241103 (2006).

[21] W.-Q. Ning, H. Zhao, C.-Q. Wu, and H.-Q. Lin, Phys. Rev. Lett. **96**, 156402 (2006).

[22] V. Meden, K. Schönhammer, and O. Gunnarsson, Phys. Rev. B **50**, 11179 (1994).

[23] M. Hohenadler, M. Aichhorn, and W. von der Linden, Phys. Rev. B **68**, 184304 (2003).

[24] M. Hohenadler, D. Neuber, W. von der Linden, G. Wellein, J. Loos, and H. Fehske, Phys. Rev. B **71**, 245111 (2005).
[25] M. Hohenadler, G. Wellein, A. R. Bishop, A. Alvermann, and H. Fehske, Phys. Rev. B **73**, 245120 (2006).
[26] M. Hohenadler, G. Wellein, A. Alvermann, and H. Fehske, Phys. B: Condens. Matter **378–380**, 64 (2006).
[27] M. Hohenadler, H. Fehske, and F. F. Assaad, Phys. Rev. B **83**, 115105 (2011).
[28] S. Sykora, A. Hubsch, K. W. Becker, G. Wellein, and H. Fehske, Phys. Rev. B **71**, 045112 (2005).
[29] G. Wellein, A. R. Bishop, M. Hohenadler, G. Schubert, and H. Fehske, Phys. B: Condens. Matter **378–380**, 281 (2006).
[30] S. Sykora, A. Hubsch, and K. W. Becker, Europhys. Lett. **76**, 644 (2006).
[31] J. Loos, M. Hohenadler, and H. Fehske, J. Phys.: Condens. Matter **18**, 2453 (2006).
[32] J. Loos, M. Hohenadler, A. Alvermann, and H. Fehske, J. Phys.: Condens. Matter **19**, 236233 (2007).
[33] C. E. Creffield, G. Sangiovanni, and M. Capone, Eur. Phys. J. B **44**, 175 (2005).
[34] M. Ogata and H. Shiba, Phys. Rev. B **41**, 2326 (1990).
[35] H. Zheng, D. Feinberg, and M. Avignon, Phys. Rev. B **39**, 9405 (1989).
[36] S. R. White and A. E. Feiguin, Phys. Rev. Lett. **93**, 076401 (2004).
[37] A. J. Daley, C. Kollath, U. Schollwock, and G. Vidal, J. Stat. Mech.: Theory Exp. (2004) P04005.
[38] R. P. Hardikar and R. T. Clay, Phys. Rev. B **75**, 245103 (2007).
[39] S. Reja, S. Yarlagadda, and P. B. Littlewood, Phys. Rev. B **84**, 085127 (2011).
[40] S. Reja, S. Yarlagadda, and P. B. Littlewood, Phys. Rev. B **86**, 045110 (2012).
[41] C. A. Perroni, V. Cataudella, G. De Filippis, and V. M. Ramaglia, Phys. Rev. B **71**, 113107 (2005).
[42] M. Hohenadler and F. F. Assaad, Phys. Rev. B **87**, 075149 (2013).
[43] A. Payeur and D. Sénéchal, Phys. Rev. B **83**, 033104 (2011).
[44] E. A. Nowadnick, S. Johnston, B. Moritz, R. T. Scalettar, and T. P. Devereaux, Phys. Rev. Lett. **109**, 246404 (2012).
[45] J. Bauer, Europhys. Lett. **90**, 27002 (2010).
[46] J. Bauer and A. C. Hewson, Phys. Rev. B **81**, 235113 (2010).
[47] S. Kumar and J. van den Brink, Phys. Rev. B **78**, 155123 (2008).
[48] P. Barone, R. Raimondi, M. Capone, C. Castellani, and M. Fabrizio, Phys. Rev. B **77**, 235115 (2008).
[49] H. Fehske, G. Hager, and E. Jeckelmann, Europhys. Lett. **84**, 57001 (2008).
[50] M. Tezuka, R. Arita, and H. Aoki, Phys. Rev. B **76**, 155114 (2007).
[51] S. Ejima and H. Fehske, J. Phys.: Conf. Ser. **200**, 012031 (2010).
[52] S. Ejima and H. Fehske, Europhys. Lett. **87**, 27001 (2009).
[53] E. Jeckelmann and S. R. White, Phys. Rev. B **57**, 6376 (1998).
[54] C. Zhang, E. Jeckelmann, and S. R. White, Phys. Rev. B **60**, 14092 (1999).
[55] V. Cataudella, G. De Filippis, F. Martone, and C. A. Perroni, Phys. Rev. B **70**, 193105 (2004).
[56] C. A. Perroni, A. Nocera, V. M. Ramaglia, and V. Cataudella, Phys. Rev. B **83**, 245107 (2011).
[57] C. A. Perroni, F. Gargiulo, A. Nocera, V. M. Ramaglia, and V. Cataudella, Electronics **3**, 165 (2014).
[58] A. Nocera, C. A. Perroni, V. M. Ramaglia, G. Cantele, and V. Cataudella, Phys. Rev. B **87**, 155435 (2013).
[59] A. Nocera, C. A. Perroni, V. Marigliano Ramaglia, and V. Cataudella, Phys. Rev. B **83**, 115420 (2011).
[60] C. A. Perroni, V. Cataudella, G. De Filippis, G. Iadonisi, V.-M. Ramaglia, and F. Ventriglia, Phys. Rev. B **67**, 214301 (2003).
[61] I. G. Lang and Y. A. Firsov, Zh. Eksp. Teor. Fiz. **43**, 1843 (1962) [Sov. Phys. JETP **16**, 1301 (1962)].
[62] K. Penc, K. Hallberg, F. Mila, and H. Shiba, Phys. Rev. B **55**, 15475 (1997).
[63] M. Soltanieh-ha and A. E. Feiguin, Phys. Rev. B **86**, 205120 (2012).
[64] M. Soltanieh-ha and A. E. Feiguin, Phys. Rev. B **90**, 165145 (2014).
[65] H. Benthien, F. Gebhard, and E. Jeckelmann, Phys. Rev. Lett. **92**, 256401 (2004).
[66] G. Mahan, *Many-Particle Physics*, Physics of Solids and Liquids (Springer, New York, 2000).
[67] S. R. Manmana, A. Muramatsu, and R. M. Noack, in *Time Evolution of One-Dimensional Quantum Many Body Systems*, AIP Conf. Proc. No. 789 (AIP, Melville, NY, 2005).
[68] P. Schmitteckert, Phys. Rev. B **70**, 121302 (2004).
[69] M.-A. Cazalilla and J.-B. Marston, Phys. Rev. Lett. **88**, 256403 (2002).
[70] M.-A. Cazalilla and J.-B. Marston, Phys. Rev. Lett. **91**, 049702 (2003).
[71] H.-G. Luo, T. Xiang, and X.-Q. Wang, Phys. Rev. Lett. **91**, 049701 (2003).
[72] T. D. Kühner and S. R. White, Phys. Rev. B **60**, 335 (1999).
[73] S. Daul and R. M. Noack, Phys. Rev. B **58**, 2635 (1998).
[74] H. J. Schulz, Phys. Rev. Lett. **64**, 2831 (1990).